Trajectory Deviations in Airborne SAR: Analysis and Compensation

G. FORNARO
IRECE-CNR
Italy

This paper concerns the analysis and compensation of trajectory deviations in airborne synthetic aperture radar (SAR) systems. Analysis of the received data spectrum is carried out with respect to the system geometry in the presence of linear, sinusoidal, and general aircraft displacements. This shows that trajectory deviations generally produce spectral replicas along the azimuth frequency that strongly impair the quality of the focused image. Based on the derived model, we explain the rationale of the motion compensation (MOCO) strategy that must be applied at the SAR processing stage in order to limit the resolution loss. To this end aberration terms are separated into range space invariant and variant components. The former can be accounted for either in a preprocessing step or efficiently at range compression stage. The latter needs a prior accommodation of range migration effect. We design the procedure for efficient inclusion of the MOCO within a high precision Scaled FT based SAR processing algorithm. Finally, we present results on simulated data aimed at validating the whole analysis and the proposed procedure.

Manuscript received March 10, 1998; revised November 4, 1998.

IEEE Log No. T-AES/35/3/06416.

Author's address: Istituto di Ricerca per l'Elettromagnetismo e i Componenti Elettronici, Consiglio Nazionale delle Ricerche, IRECE-CNR, Via Diocleziano, 328 I-80124 Napoli, Italy; E-mail: (fornaro@irece1.irece.na.cnr.it).

I. INTRODUCTION

Synthetic aperture radar (SAR) is a remote sensing system used to obtain high-resolution microwave images of the observed scene. The device is mounted on-board a platform (airplane, satellite or Space Shuttle) that, in the ideal case, moves with a constant (forward) velocity along a rectilinear trajectory. The scene is illuminated at constant time intervals and the received signal (raw data) contains information about its backscattering properties at the microwave frequencies.

High geometric resolution in range (target to flight path distance) is obtained via transmission of large bandwidth pulses. On the other hand, high resolution in azimuth (flight direction) is the result of an intensive coherent data processing (focusing or pulse compression) operation aimed at synthesizing an antenna array whose dimension is several times (10^2–10^3) larger than the one of the real illuminating antenna mounted on-board the platform [1]. Moreover, in order to limit the transmitted pulse peak power, most of the SAR systems achieve high bandwidths by transmitting (long duration) linearly frequency modulated (chirp) pulses. Accordingly, digital processing for pulse compression is usually required also in range direction to compensate the induced chirp phase distortions [1].

Azimuth and range pulse compression, through match filtering, is generally carried out in the frequency domain and accounts for intrinsic space variant effects such as focus depth and range cell migration (RCM) [1]. With this regard, efficient techniques referred to as Chirp Scaling (CS) [2] and Scaled Fourier Transform (SC-FT) [3,4] SAR processing have been presented in literature. They are compared in [5] and address the problem by assuming the ideal trajectory case.

In airborne SAR systems deviations of the trajectory from the nominal one as well as attitude and forward velocity variations frequently occur mainly due to atmospheric turbulence. These introduce motion errors on the received raw data that, beside the loss of geometrical accuracy, may strongly impair the final image quality in terms of geometric and radiometric resolution losses if not properly accounted for during the processing [6, 7]. To compensate for motion errors, flight information must be available at the raw data processing stage. Usually these are provided by inertial navigation units (INU) and Global Positioning System (GPS) mounted on-board the airplane [8]. Alternatively, motion errors may be directly estimated from the raw data by means of the reflectivity displacement method (RDM) [9], autofocus [10–12], and phase-retrieval [13] techniques. A discussion on autofocus techniques and in general on image defects and their correction can be found in [14].

Motion compensation (MOCO) procedures that account for known deviations of the flight trajectory during the SAR processing have been proposed in the past years. A simple method can be implemented by assuming that trajectory deviations introduce a space invariant aberration thus generating a phase modulation and shifting of the received data that only varies with the platform position. The MOCO procedure reduces in this case to a phase multiplication and a range gate adjustment that can be addressed in a preprocessing step [15, 16]. Unfortunately the space invariance assumption is not satisfactory for high-resolution airborne SAR systems [17]. Processing algorithms that account for additional space variant aberrations have been also proposed [17–19]. In [17] impossibility in coupling target RCM and space-variant (second-order) motion compensation is heuristically recognized, but no analytical justification can be found: operating with time-consuming high amount of raw data segmentation during the processing step circumvents this problem. In [18, 19] the algorithm accounts for second-order MOCO after the RCM compensation. However, the rationale of the processing chain with respect to this problem is insufficiently detailed.

Forward velocity and attitude variations induce additional image quality degradation [6]. The former causes a spatial variation between the elements of the synthetic antenna array and may be compensated, if spectral aliasing effects are negligible, via a proper resampling of the received raw data in azimuth direction. The latter, which mainly generate radiometric resolution loss, may be either eliminated by serving the real antenna to a fixed look direction or compensated by knowing the illumination characteristics of the transmitting antenna at the image calibration stage [6].

This work carries out the analysis of the motion error effects by evaluating the spectrum of the received raw data in the presence of trajectory displacements. Forward velocity and attitude variations are not dealt with; they are presumed to be absent or possibly compensated as explained before. It is shown (in Section III) that in general a continuous replication along the azimuth frequency of the raw data spectrum obtained in absence of deviation is present; replicas are weighted and integrated according to the spectrum of the phase aberration term due to the trajectory displacement.

To analyze the effects of such frequency replication, relevant cases of linear and sinusoidal displacements are subsequently addressed. In the former case a single spectral replica is present thus introducing a limited degradation that could be handled at the processing stage. The latter generate a more significant spectral degradation: the received spectrum is a discrete summation of replicas weighted accordingly to Bessel function coefficients that are dependent upon the amplitude and frequency of the sinusoidal trajectory deviation. As a consequence, after the processing, the desired target response is attenuated according to the coefficient pertinent to the fundamental replica; moreover additional *paired echoes*, which may even be dominant, appear along the azimuth direction thus strongly impairing the image quality.

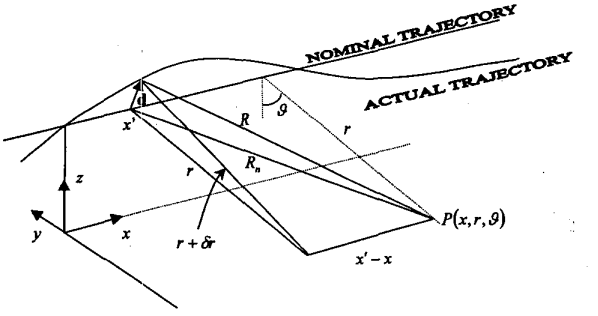

Fig. 1. SAR system geometry in presence of trajectory deviation.

Section IV continues with the explanation of the MOCO strategy that must be implemented during the SAR processing in order to limit the image quality degradation induced by the platform deviations. Aberration terms are separated into range space invariant and variant components. It is shown that the former can be accounted for either in a preprocessing step or more efficiently at the range compression stage, the latter requires a preliminary accommodation for the range migration effect. A high precision SC-FT based SAR processing algorithm with integrated MOCO is presented and tested on simulated data in Section V. In comparison to the one proposed in [18, 19], which refers to a CS SAR processing algorithm, the proposed method achieves the same computational efficiency and retains the advantages of SC-FT based SAR processors: flexibility with respect to the transmitted waveform and absence of any approximation in the range independent RCM [5] compensation. It is important to note that, beside these interesting aspects of the implemented code, this work does not address a new motion compensation strategy. Indeed, it contains a sound mathematical formalization of the trajectory displacement problem in airborne SAR systems, which allows analysis of the image quality degradation and fully explains the rationale of MOCO strategies.

II. RAW DATA IN PRESENCE OF TRAJECTORY DISPLACEMENTS

Let us refer to Fig. 1 in which the SAR system geometry in the presence of trajectory displacement is shown: (x,r) are the azimuth and (slant) range coordinate of the generic scene scatter P in a

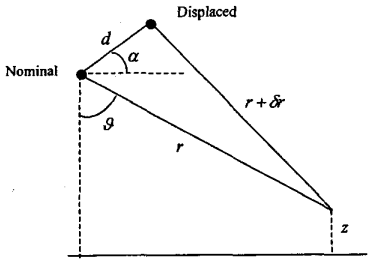

Fig. 2. SAR system geometry in cross (nominal) track plane.

cylindrical reference system. The reference system axis coincides with the nominal trajectory; x' is the position of the illuminating antenna, $\mathbf{d}$ is the displacement vector whose y and z components are the horizontal and vertical platform displacements (x component is supposed to be null or compensated as explained in Section I); δr is the range displacement in the plane orthogonal to the flight direction; R and R_n are the target-to-antenna distance in the generic antenna position with respect to real and nominal trajectory, respectively. Absence of any squint angle is assumed and the illuminated surface is supposed flat.

From Fig. 1 we have the following expressions for R and R_n:

$$R_n(r,x'-x) = \sqrt{r^2 + (x'-x)^2} \quad (1)$$

$$R(r,x',x) = \sqrt{(r+\delta r)^2 + (x'-x)^2}. \quad (2)$$

The δr term depends on x' and r, and can be evaluated by the application of the Carnot Theorem (see also Fig. 2) as follows:

$$\delta r(x',r) = \sqrt{r^2 + d^2 - 2dr\sin(\vartheta - \alpha)} - r \approx -d\sin(\vartheta - \alpha). \quad (3)$$

where $d(x')$ and $\alpha(x')$ are related the horizontal and vertical platform displacements; $\vartheta(r)$ is the target look angle. The last approximation in (3) holds when displacements are small compared with the target slant range; δr reduces in this case to the displacement projection onto the target look direction.[1]

Assume now that the transmitted signal has the following expression (chirp pulse):

$$f(t') = rect\left[\frac{t'}{\tau}\right]\exp\left(j2\pi f_0 t' - j\frac{\alpha_t}{2}t'^2\right) \quad (4)$$

where f_0 is the carrier frequency, τ and α_t are the chirp duration and rate, respectively. After heterodyne we have the following expression for the collected (raw) signal [1]:

$$hh(x',r') = \iint dx\,dr\,\gamma(x,r) \times \exp\left(-j\frac{4\pi}{\lambda}R - j\alpha_r(r'-R)^2\right) \times \text{rect}\left[\frac{r'-R}{D_r}\right] w^2(x'-x) \quad (5)$$

wherein $r' = ct'/2$ is the range signal sampling coordinate, α_r and D_r are the spatial counterparts of α_t and τ; $\gamma(\cdot)$ is the signal which models the backscattering scene properties (i.e., the signal we want to estimate) in the cylindrical reference system, and $w(\cdot)$ is the antenna ground illumination pattern which is usually approximated to rect$[(x'-x)/X]$; X is the synthetic antenna length.

Spectral analysis of degradation induced in (5) by the presence of $R(r,x',x)$ rather than $R_n(r,x'-x)$ is now addressed.

III. FREQUENCY DOMAIN ANALYSIS

Equation (5) can be transformed in range direction thus obtaining [1]

$$hH(x',\eta) = \text{rect}\left[\frac{\eta}{2\Omega_r}\right]\exp[j\alpha_\eta\eta^2] \times \iint dx\,dr\,\gamma(x,r)w^2(x'-x) \times \exp[-j(\eta + 4\pi/\lambda)R] \quad (6)$$

where $\Omega_r = \alpha_r D_r$ and $\alpha_\eta = 1/4\alpha_r$.

Equation (6) has the same expression of the raw data range spectrum obtained in the absence of platform deviations, but for the presence of R in place of R_n. The η^2 dependence in the first exponential term highlight the phase distortion induced by the transmitted chirp signal; moreover, should R be substituted by R_n, we would recognize in (6) the typical azimuth frequency modulation (η-independent) and the target RCM (η-dependent) terms in the second exponential factor.

We now expand R as follows:

$$R(x-x,x',r) = R_n(x'-x,r) + \delta R(x'-x,x',r) \quad (7)$$

where:

$$\delta R \approx \frac{\partial R}{\partial \delta r}\delta r = \frac{r}{R_n}\delta r(x',r) \approx \delta r - \frac{(x'-x)^2}{2r}\frac{\delta r}{r}. \quad (8)$$

In the following we suppose

$$\frac{X^2}{2r}\frac{|\delta r|}{r} \ll \frac{\lambda}{4\pi}$$

thus neglecting the last factor in (8) as far as substitution in (6) is concerned. This corresponds to assuming (see again Fig. 1) that the azimuth beam

[1]Equations (1)–(3) are very similar to those pertinent to interferometric SAR systems [17, 20].

is narrow enough to consider, for a generic sensor position x', the displacement error (δR) for all the targets within the beam (in azimuth direction) equals the one of the center beam (zero Doppler) target ($x = x'$):

$$\delta R(x' - x, x', r) \approx \delta r(x', r). \tag{9}$$

This important assumption, together with the flat surface hypothesis, involves the elimination of any displacement error space variance over the target azimuth coordinate (x) and allows the further interesting developments in the following spectral analysis. Furthermore, it should be noted that this azimuth (target-dependent) space variance would be extremely difficult to handle at the data processing stage for SAR focusing algorithms operating in the spectral domain.

Equation (6) can now be transformed along the azimuth direction (x'). We get (see appendix)

$$HH(\xi,\eta) = \frac{1}{2\pi}\int dr \exp[-j(\eta + 4\pi/\lambda)r] \times \int d\zeta Q(\zeta,\eta,r)\Gamma(\xi - \zeta, r)G(\xi - \zeta,\eta,r) \tag{10}$$

where $G(\xi,\eta,r)$ is the SAR system transfer function (STF) pertinent to the ideal trajectory case, and $\Gamma(\xi,r)$ is the FT of $\gamma(\cdot)$ along x, and

$$Q(\xi,\eta,r) = FT_{x'}\{q(x',\eta,r)\}, q(x',\eta,r) = \exp[-j(\eta + 4\pi/\lambda)\delta r(x',r)] \tag{11}$$

is the azimuth FT of the aberration term induced by the trajectory displacement. Dependence of $G(\cdot)$ upon the target range r, highlights the usual range space variant character of the SAR STF due to the focus depth and range-dependent RCM (RD-RCM) effects [1–4].

Equation (10) is of fundamental importance in the following analysis. It is trivial to recognize that, in the absence of trajectory displacements we have $Q(\xi,\eta,r) = 2\pi\delta(\xi)$, where $\delta(\cdot)$ is the Dirac impulse function, thus retaining the standard spectral expression of the received raw data [1, 3]:

$$HH_n(\xi,\eta) = \int dr \exp[-j(\eta + 4\pi/\lambda)r]\Gamma(\xi,r)G(\xi,\eta,r). \tag{12}$$

Discussion about differences between (10) and (12) is addressed in the following. To have a better insight into this problem we preliminary analyze the two particular cases of linear and sinusoidal trajectory deviation.

A. Linear Trajectory Displacement

Let us consider a linear trajectory displacement which can be due to the presence of a constant cross track velocity component. We get from (3)

$$\delta r \approx a(r)x'. \tag{13}$$

Equation (10) simplifies in this case as follows:

$$HH(\xi,\eta) = \int dr \exp[-j(\eta + 4\pi/\lambda)r] \times \Gamma(\xi - \xi_0, r)G(\xi - \xi_0,\eta,r) \tag{14}$$

where $\xi_0(\eta,r) = (\eta + 4\pi/\lambda)a(r)$.

Equation (14) shows that linear trajectory displacements translate in spectral shift along the azimuth direction of the SAR STF thus generating a limited degradation.[2] This is in complete agreement with the fact that SAR, for rectilinear trajectories, is sensitive to relative target-to-platform distances no matter how the former is oriented. The azimuth spectral shift of the SAR STF is usually referred to as Doppler Centroid and is pertinent to squinted geometry [1–3]. Here, the squint is apparent being the reflectivity spectrum shifted of the same quantity; see (14).

However, it must be noted that dependence of $\xi_0(\cdot)$ over η and r (this latter is not accessible for SAR focusing algorithms operating in the frequency domain) account for geometric distortions [6] that are present when deviations occur and geometry is fixed with respect to the nominal trajectory. Precise geometric correction,[3] which in general depends also on the scene topography, is difficult to handle at processing stage unless simplifying approximations on r dependence are carried out [20]. Accordingly, for general aircraft deviations, to limit the effects of these unavoidable approximations in the geometric correction, the nominal trajectory should be in any case chosen in such a way as to minimize the trajectory deviations, possibly by proper data segmentation along the azimuth direction.

As a last remark, we note that spectral shifting is dependent on $a(r)$ that is related to the cross track velocity component projected onto the slant range plane. In case of general trajectory displacement, this latter varies over the azimuth coordinate. Should this variation be sufficiently slow, a method to estimate it from the raw data could be implemented [9] by correlating, in azimuth direction, spectra relative to strong overlapping azimuth data segments.

---

[2]Note that in the adopted hypothesis the real antenna is in any case pointing orthogonal to the nominal trajectory.

[3]In [20] this geometric correction is deeply investigated with reference to the image registration in Interferometric SAR processing which may be considered equivalent to a very simple deviation compensation problem with parallel nominal and real trajectories. The latter are associated to the master and slave orbits of the Interferometric system, respectively.

TABLE I
Simulated Sensor Parameters

Nominal height	3000 m	Sampling frequency	100 MHz
Scene center look angle	52.993°	Chirp bandwidth	90 MHz
Synthetic aperture length	180 m	Chirp duration	5 μs
Nominal velocity	80 m/s	Wavelength	3.14 cm
Pulse Repetition Frequency	250 Hz	Range delay	23 μs
Azimuth pixels	2048	Range pixels	2048

B. Sinusoidal Trajectory Displacement

Let us now suppose that trajectory deviations are described by a sinusoidal function. Therefore we let

$$\delta r = a(r)\sin(\xi_0 x') \tag{15}$$

wherein $a(r)$ is the amplitude sinusoidal deviation projected over the slant range plane.

Expansion of $q(\cdot)$ in (11) can be carried out by use of Bessel function, thus obtaining [21]

$$q(x',\eta,r) = \sum_{k=0}^{+\infty} j^k J_k(A)\cos(k\xi_0 x' + k\pi/2) \tag{16}$$

where $J_k(A)$ is the kth-order first kind Bessel function and $A(\eta,r) = (\eta + 4\pi/\lambda)a(r)$.

Substitution of the azimuth FT of (16) in (10) leads to

$$HH(\xi,\eta) = \int dr \exp[-j(\eta + 4\pi/\lambda)r] \sum_{k=-\infty}^{+\infty} C_k j^{|k|} J_{|k|}(A) \times \Gamma(\xi - k\xi_0, r) G(\xi - k\xi_0, \eta, r)\exp[jk\pi/2] \tag{17}$$

wherein, $C_0 = 1$ and $C_k = 1/2$ for $k \neq 0$.

But for the approximation in (9), (17) describes the exact expression of the raw data spectrum. Only to interpret (17) we do carry out some simplifying approximations. First of all we note that, generally $4\pi/\lambda \gg \Omega_r$, therefore the η dependence of $A(\cdot)$ can be neglected. Secondly, we suppose that the range variation of $A(\cdot)$ is also negligible by letting $r = r_0$, where r_0 is the range coordinate of the scene center. Accordingly, (17) simplifies to

$$HH(\xi,\eta) = \sum_{k=-\infty}^{+\infty} C_k j^{|k|} J_{|k|}(A(0,r_0)) \times \exp[jk\pi/2] HH_n(\xi - k\xi_0, \eta). \tag{18}$$

Equation (18) states that, in the case of sinusoidal deviation, the raw data spectrum consists of a (discrete) summation, along the azimuth frequency, of shifted versions of the spectrum pertinent to the ideal trajectory; the summation is weighted by the Bessel function coefficients (Fig. 3). The higher the amplitude of the sinusoidal displacement, the larger the number of significant replicas in (18) according to the coefficients described by the Bessel functions [21, 22].

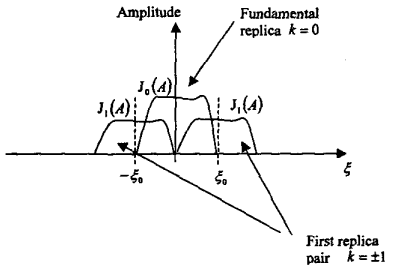

Fig. 3. Spectral replication of received raw data along azimuth frequency induced by sinusoidal deviations.

At this stage, if processing is performed on the received raw data by use of the standard STF, i.e., the filter matched to the fundamental replica ($k = 0$) [1–3], aberrations arise in the final image. First of all, the desired target response is attenuated by the factor $J_0(A)$. Moreover, matches between the STF and remaining significant replicas, which can be emphasized by the relative Bessel function coefficients, generate paired echoes[4] at the azimuth positions $x \pm (\lambda/4\pi)k\xi_0 r$. Amplitude of the echoes depends upon the weighting factors $J_k(A)$. Spatial separation is related to the frequency of the sinusoidal deviation.

To highlight this effect we present an experimental result carried out on simulated data whose sensor parameters are collected in Table I. A target has been located at the image center, $r_0 = 4984$ m, and trajectory has been displaced along the y direction with sinusoidal deviation of 1 cm amplitude and 16.5 cycles per synthetic aperture length frequency; the azimuth flight time is of 8.19 s. Accordingly, we have $\xi_0 = 0.57$ rad/m and, via (3), $A(0,r_0) = 3.2$. Note that, although such motion errors are never encountered in real airborne SAR systems, high frequency of the sinusoidal deviation has been chosen in the presented simulation to emphasize the spectral separation between the replicas; low amplitude limits the number of significant Bessel coefficients [21, 22].

Fig. 4 shows the spectrum $Q(\xi,0,r_0)$ while in Fig. 5 we plot the azimuth target response after the

[4]Note that from (18) replicas are always present as pairs.

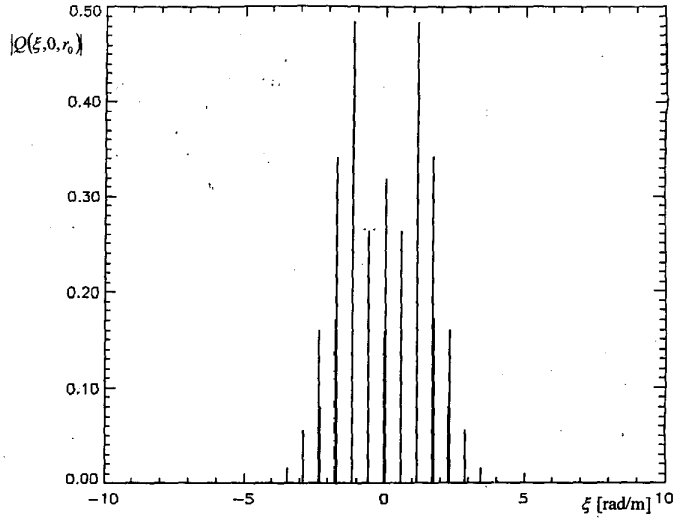

Fig. 4. Amplitude spectrum of aberration term $|Q(\xi,0,r_0)|$ for sinusoidal trajectory deviation simulated case.

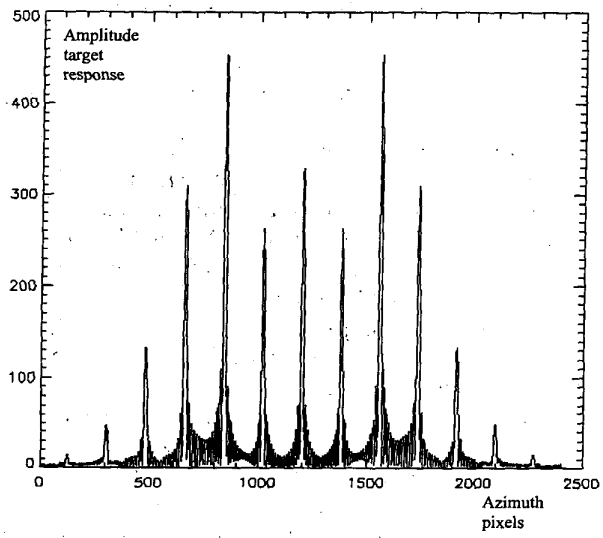

Fig. 5. Azimuth degradation of impulse response function: presence of sinusoidal deviation attenuates target response and induces additional paired echoes that are scaled in amplitude in accordance with spectrum in Fig. 4.

SAR focusing operation (2400 central samples). It is evident that the desired target response has been attenuated according to $J_0(A)$, while paired echoes corresponding to $k = \pm 2, \pm 3$ are predominant. From the parameter in Table I we get an echo separation $((\lambda/4\pi)k\xi_0 r_0)$ of 22.2 pixels. The spacing between the echoes in Fig. 5 is 178 samples which is congruent with the theoretical value by considering that an over-sampling factor of 8 has been used in Fig 5.

Let us now address the case of general deviations. Equation (10) is in this case the continuous counterpart of (17). Neglecting, as in the sinusoidal case, η and r dependencies of $Q(\cdot)$, we have

$$HH(\xi,\eta) = \int d\zeta Q(\zeta,0,r_0) HH_n(\xi-\zeta,\eta). \tag{19}$$

In this case the raw signal spectrum consists of a continuous summation of replicas weighted by the spectrum of the deviation-induced term $Q(\cdot)$. Replicas that fall out of the spectral extent of $Q(\xi,0,r_0)$, say Ω_q, are strongly attenuated. On the other hand, in bandwidth, replicas generate, after the focusing step, a continuum of echoes in azimuth direction that cause a strong resolution degradation. For instance, in analogy to the sinusoidal case, a measure of the azimuth target dispersion is given by

$$\Delta x_d = \frac{\lambda}{4\pi}\Omega_q r. \tag{20}$$

A last remark is now dedicated to a discussion about the quoted approximations on η and r dependence of $Q(\cdot)$ that have been introduced to carry out an easy interpretation of (10) and (17). Strictly speaking these are valid only if $q(\cdot)$ in (11) can be approximated to

$$q(x',\eta,r) \approx \exp[-j(4\pi/\lambda)\delta r(x',r_0)] = q(x') \tag{21}$$

that is, if trajectory displacements are small enough to consider $\Omega_r|\delta r(x',r)| \ll 1$ and $|\delta r(x',r) - \delta r(x',r_0)| \ll \lambda/4\pi$. In the real case these conditions are rarely satisfied; r dependence account for the fact that trajectory displacement projection over the slant range plane, see (3), is dependent upon the target look angle. On the other hand, the η dependence accounts for the fact that the targets responses are mislocated in range with respect to those obtained in the absence of trajectory deviations. These generate, as discussed in Section IIIA, image geometric distortion [6] and an additional range variant spreading of the echo

responses generated by the continuous or discrete *replicas, thus* further impairing the image quality.

IV. PROCESSING PROCEDURE

Suppose now that trajectory displacement is measured by an INU and available at the SAR processing stage. We are now interested in the motion error compensation problem to limit the azimuth resolution loss. To this end it is convenient to separate δr into range space invariant (at the scene center) and variant contributions as follows:

$$\delta r(x',r) = \delta r_0(x') + \delta r_v(x',r) \tag{22}$$

where $\delta r_0(x') = \delta r(x',r_0)$. These terms are computable from (3) by knowing the trajectory deviations. From the expression of the range FT of the received raw data, (6), we have

$$hH(x',\eta) = \text{rect}\left[\frac{\eta}{2\Omega_r}\right] \exp[j\alpha_\eta \eta^2 - j(\eta + 4\pi/\lambda)\delta r_0] \times \iint dx\,dr\,\gamma(x,r)w^2(x'-x) \times \exp[-j(\eta + 4\pi/\lambda)(R_n + \delta r_v)]. \tag{23}$$

We again recognize in (23) typical terms of the SAR STF [1, 3]. The $4\pi/\lambda(R_n - r)$ phase term is the azimuth ideal target phase response (approximately a chirp) including the focus depth term ($r \neq r_0$); the $\eta(R_n - r)$ phase term accounts for the target range-independent ($r = r_0$) and range-dependent ($r \neq r_0$) RCM.

A. Bulk Motion Compensation

Compensation of the term $\exp[-j(\eta + 4\pi/\lambda)\delta r_0]$, referred to as bulk or first-order MOCO, requires a phase correction, i.e., multiplication by $\exp[j(4\pi/\lambda)\delta r_0]$, and repositioning of the raw data in range direction. Being δr_0 independent on the slant range coordinate r, the bulk MOCO could be addressed in a preprocessing step. However, to optimize the efficiency of the processing procedure we can directly perform it at the range compression stage. This is carried out via a multiplication of (23) by $\exp[-j\alpha_\eta \eta^2 + j(\eta + 4\pi/\lambda)\delta r_0]$.

The obtained signal, which for the sake of simplicity we continue to refer to as $hH(x',\eta)$ may be now transformed back in the space domain for further consideration. We have

$$hh(x',\eta) = \iint dx\,dr\,\gamma(x,r)w^2(x'-x) \times \exp\left[-j\frac{4\pi}{\lambda}(R_n + \delta r_v)\right] \times \text{sinc}[\Omega_r(r' - r - (R_n - r))] \tag{24}$$

where we neglect the presence of the residual response displacement, δr_v, within the $sinc(\cdot)$ function by using R_n instead of $R_n + \delta r_v$.

B. Residual Motion Compensation in Negligible Range Migration Case

Let us now address the problem of the residual (range space variant) displacement error (δr_v) compensation. To this end we first consider SAR system with negligible range migration. In other words we suppose, see (23), that

$$\Omega_r(R_n - r) \ll \pi. \tag{25}$$

Equation (24) simplifies in this case as follows:

$$hh(x',\eta) = \iint dx\,dr\,\gamma(x,r)w^2(x'-x) \times \exp\left[-j\frac{4\pi}{\lambda}(R_n + \delta r_v)\right] \text{sinc}[\Omega_r(r' - r)]. \tag{26}$$

For a large transmitted bandwidth, we can consider $\delta r_v(x',r)$ constant within the pixel, i.e., in $|r' - r| < \pi/\Omega_r$, thus obtaining

$$hh(x',\eta) \approx \exp\left[-j\frac{4\pi}{\lambda}\delta r_v(x',r')\right] \times \iint dx\,dr\,\gamma(x,r)w^2(x'-x) \times \exp\left[-j\frac{4\pi}{\lambda}R_n\right] \text{sinc}[\Omega_r(r' - r)]. \tag{27}$$

Compensation of the residual motion error term (second order MOCO) is simply carried out via a phase multiplication by

$$\exp\left[j\frac{4\pi}{\lambda}\delta r_v(x',r')\right].$$

Azimuth compression, i.e., compensation of the phase term

$$\exp\left[-j\frac{4\pi}{\lambda}(R_n - r)\right]$$

is at this stage the last processing step and can be performed via a couple of one-dimensional azimuth transform [1, 3].

The problem of residual motion error compensation is therefore easily solved in the case of negligible range migration system. Unfortunately, most of the SAR systems do not satisfy condition (25). Accordingly, the $\delta r_v(x',r)$ phase term cannot be singled out from the integral in (24).

C. Residual Motion Compensation in Nonnegligible Range Migration Case

Similar to the derivation of (10), the FT of the signal in (24) in range (r') and azimuth (x') directions

gives

$$HH(\xi,\eta) = \text{rect}\left[\frac{\eta}{2\Omega_r}\right]\int dr \exp\left[-j\left(\frac{4\pi}{\lambda}+\eta\right)r\right] \times \int d\zeta Q_v(\zeta,r)\Gamma(\xi-\zeta,r)G_x(\xi-\zeta,\eta,r) \tag{28}$$

where $G_x(\xi,\eta,r)$ is now the standard SAR STF after the range compression step, and nonessential amplitude factors have been neglected. Moreover, due to the fact that range-invariant displacement errors have been already compensated, we have

$$q_v(x',r) = \exp[-j(4\pi/\lambda)\delta r_v(x',r)] \tag{29}$$

which, according to the approximation on the residual displacement within the sinc(·) function in (24), is no longer η-dependent.

For the following analysis we need to detail the expression of $G_x(\xi,\eta,r)$, that may be evaluated via the phase stationary approach. We have [1, 3, 4]:[5]

$$G_x(\xi,\eta,r) = G_1(\xi,\eta,r)G_2(\xi,\eta,r) \tag{30}$$

$$G_1(\xi,\eta,r) \approx w^2\left(\frac{\xi}{2\Omega_x}\right)\text{rect}\left[\frac{\eta}{2\Omega_r}\right]\exp\left[-j\frac{\xi^2}{2}\frac{\lambda r}{4\pi}\right] \tag{31a}$$

$$G_2(\xi,\eta,r) \approx \exp\left[j\frac{\xi^2}{2}\frac{\lambda r}{4\pi}\frac{\eta\lambda}{4\pi}\right]. \tag{31b}$$

In (30) $G_1(\xi,\eta,r)$ accounts for the azimuth frequency modulation including the focus depth effect; $G_2(\xi,\eta,r)$ is the term describing the target RCM, $2\Omega_x = 4\pi/L$ is the SAR azimuth bandwidth where L is the azimuth dimension of the real illuminating antenna.

For moderate trajectory displacement, as far as the range migration term is concerned, we can suppose $Q_v(\xi,r)$, which is the FT of the residual displacement phase aberration, is *sufficiently* low dispersion along ξ, in the sense that

$$\int d\zeta Q_v(\zeta,r)\Gamma(\xi-\zeta,r)G_x(\xi-\zeta,\eta,r) \approx G_2(\xi,\eta,r)\int d\zeta Q_v(\zeta,r)\Gamma(\xi-\zeta,r)G_1(\xi-\zeta,\eta,r). \tag{32}$$

Note that, since usually $\eta\lambda/4\pi \ll 1$, this is a sound approximation only for the factor $G_2(\cdot)$, which varies slowly with respect to $G_1(\cdot)$. Moreover, we note that this approximation takes benefit from the fact that the space-invariant displacement error has already been compensated in the bulk motion compensation step thus rendering the Q_v ξ-bandwidth much lower than the one of Q in (10). The simulation result of the next section confirms the limited effects of this important approximation.

[5]Note that to simplify the analysis, we use an approximate expression of the SAR STF; a more precise relationship, also used in the implemented MOCO code, can be found in [3].

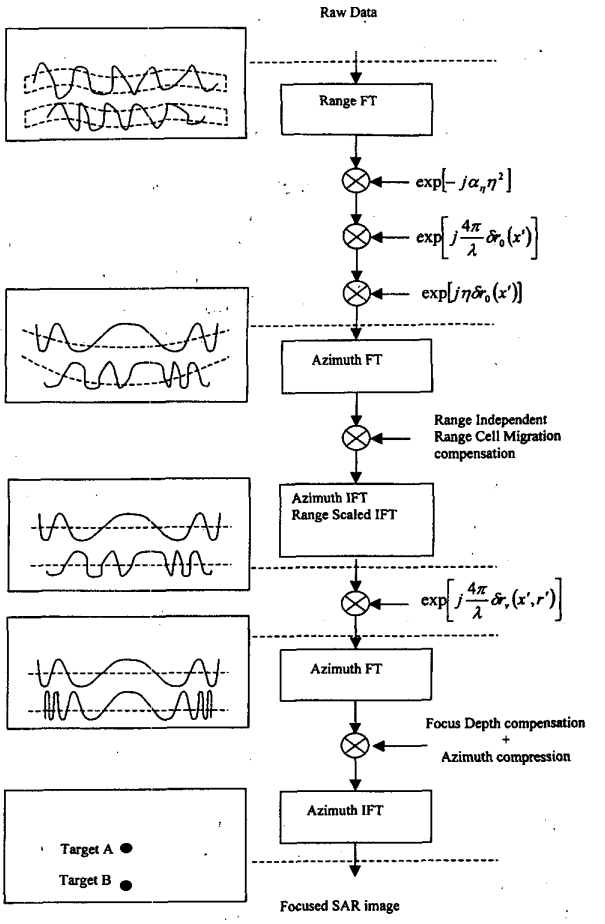

Fig. 6. Block diagram of proposed Scaled-FT based SAR processor with integrated motion compensation.

Equation (32) shows that the range migration filter component in $G_x(\cdot)$ can be singled out from the deviation-induced convolution integral in (28). At this stage target RCM correction is implemented via multiplication of the signal in (28) by $G_2^*(\xi,\eta,r_0)$ in the frequency domain [1] and a range scaled inverse FT which can be carried out via SC-FT procedures [3, 4, 20]. Additional azimuth inverse FT leads to the signal in (26). Remaining processing follows at this stage the strategy described in the negligible range migration case (Section IVB).

The block diagram of the proposed SC-FT SAR processing with integrated MOCO is shown in Fig. 6. We also show the compensation effects in the image domain for two point targets: point target A is located at the image center while B is in the near range; amplitudes are dotted while phases are continuous lines.

The raw data, possibly resampled to a constant azimuth spacing to account for forward velocity variations, are first transformed in range direction where, coupled to the range chirp compression, the bulk MOCO is carried out. Additional azimuth

transformation is performed to compensate the target range migration with respect to the scene center. Azimuth and range inverse FT are therefore carried out; the latter is a scaled one to accommodate the residual range migration effect [3, 4, 20]. At this stage the second order motion term is compensated and a final filtering is considered to perform a precise azimuth compression that includes compensation of the focus depth effect.

With respect to the standard SC-FT based high precision SAR processing [3, 4, 20], MOCO is fully implemented in the proposed algorithm with only two additional (one-dimensional) azimuth FTs.

A final remark is dedicated to a comparison between the proposed method and those presented in [17–19]. In [17] the problem of the second order MOCO in presence of significant RCM is circumvented via a strong segmentation of the raw data. In this way the real trajectory is better approximated by local rectification thus reducing the influence of motion aberration terms. However, the computational efficiency is strongly impaired by the high amount of segments that need to be processed. To carry out a comparison between the proposed method and the one presented in [18, 19] which is based on a CS SAR processing algorithm [2] we need to summarize shortcomings of both CS and SC-FT SAR processing procedures. As presented in [5], the CS based SAR processor achieves the best computational efficiency (two FTs less) with respect to the SC-FT based one. This is, however, obtained at the expense of the requirement that the transmitted signal is a chirp, and of a second order truncation on the Taylor expansion of the range independent component of the RCM in the SAR STF. These two conditions allow the compensation of the RCM in CS-SAR processing algorithms as a first step by means of an appropriate phase multiplication in the range-Doppler domain, i.e., the (ξ, r') domain. With respect to the basic procedure of [2], integration of the MOCO [18, 19] requires two additional FT in azimuth for the compensation of the second order MOCO, and two additional FT in range for the subpixel range repositioning in the first-order MOCO.[6] By comparing number of FTs required in the integration of MOCO in the CS and the proposed algorithm we conclude that the two procedures achieve the same computation efficiency; however, the latter does not have the before-mentioned limitations.

V. SIMULATION RESULTS

This section presents the experimental results regarding the processing procedure discussed in Section IV. All the results are carried out by processing simulated data: sensor parameters are again the one of Table I. Raw data relative to 5 point targets have been simulated by introducing a 0.42 cycles per synthetic aperture length frequency and 3 m amplitude sinusoidal trajectory deviation along the y direction. The location of the target has been chosen in order to separately test the performance of the space invariant and variant motion compensation, central range is of 4984 m, while near and far range target are at 3898 m and 6118 m, respectively.

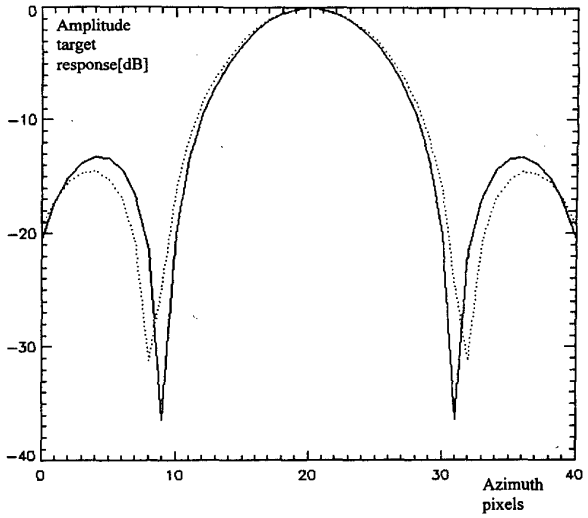

Fig. 7. Azimuth cut of nominal target response with (continuous line) and without (dotted line) range migration correction.

The simulated SAR system is sensitive to range migration effects: in Fig.7 we plot the azimuth response after the SAR processing with and without range migration compensation in nominal conditions for one target.

On the other hand, the introduced motion errors are also severe; we have from (3)

$$A(0, r_0) = \frac{4\pi}{\lambda} d_{\max} \sin(\vartheta_0) = 959$$

and $Q(\cdot)$ in (19) cover the whole available azimuth bandwidth. In Fig. 8, the image obtained in absence of any motion compensation is shown. It is evident the target azimuth dispersion, which even render it extremely difficult to localize the three center range targets. Theoretical azimuth dispersion given by (20) with Ω_d equals to the available azimuth bandwidth, gives 598 and 938 samples for the near and far range target, respectively, which are in complete agreement with the measured values in the image of Fig. 8.

Fig. 9 presents the image obtained by compensating only the space invariant term $\delta r_0(x')$: targets in the image center are perfectly focused at variance with those located in the near and far range which are sensibly degraded.

[6]Note that in [18, 19] the latter FTs are implicitly included in the preprocessing step.

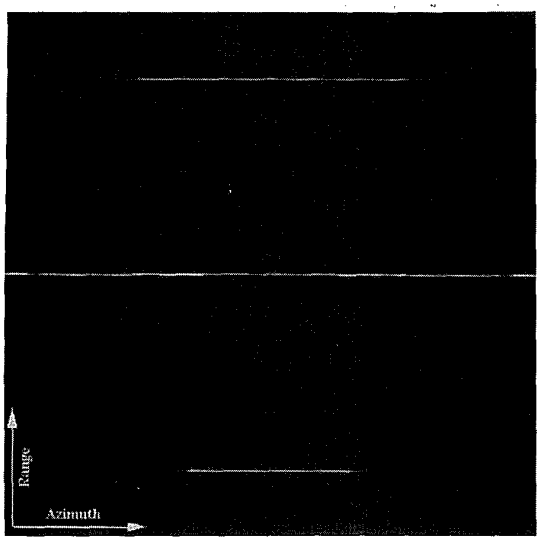

Fig. 8. Image processed without MOCO.

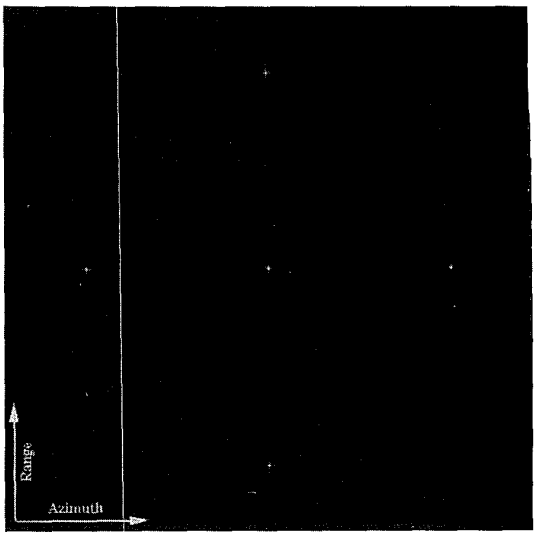

Fig. 10. Image processed with compensation of space-invariant and variant terms.

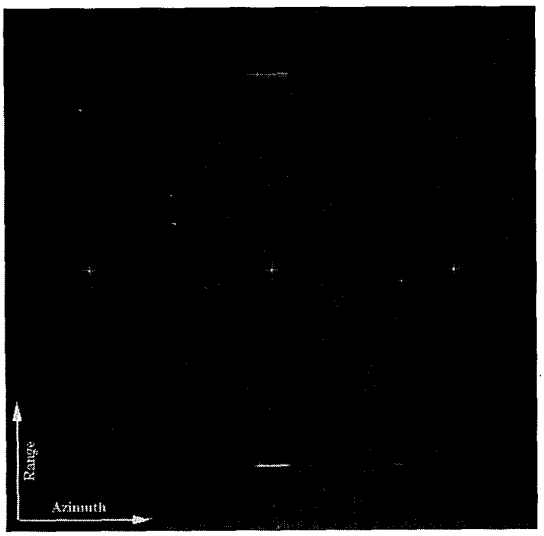

Fig. 9. Image processed by compensating only space-invariant motion-induced term.

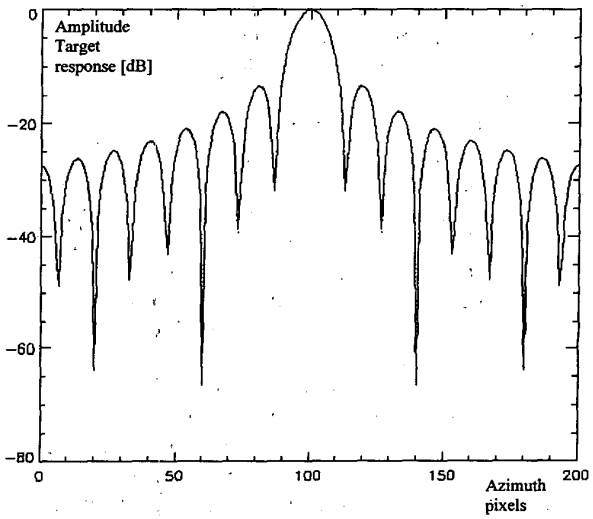

Fig. 11. Azimuth cut of nominal (continuous line) and motion compensated (dotted line) far range target response.

Compensation of the space variant motion error $\delta r_v(x',r)$ is now tested. Fig. 10 is the result obtained by applying the processing procedure of Fig. 6: benefits of the space variant motion compensation are evident on the near and far range targets. Three azimuth cuts of the image in Fig. 10 for the far, center, and near range are depicted in Figs. 11, 12, and 13, respectively, together with the one obtained in the absence of deviations. Differences in the compensated and nominal responses for far and center range targets are not detectable while the near range target shows a slight degradation in terms of resolution and peak sidelobe ratio.

To explain this degradation, tests on the effects induced by the approximation in (32) for this specific data have been carried out. In Figs. 14 and 15 we plot the phase of the ratio between the left and right-hand side terms in (32) within the system bandwidth (phase distortion) for the far and near range target, respectively; range frequency is relative to the worst case, i.e., $\eta = \Omega_r$. Amplitude distortions of the quoted ratio have been measured within 0.6 dB and maximum at the bandwidth limits. It is evident that phase distortions are more pronounced for the near range target. This, in addition to the fact that approximation in (9) is much more critical in near range, justify the slight degradation of the compensated response for the near range target in Fig. 13.

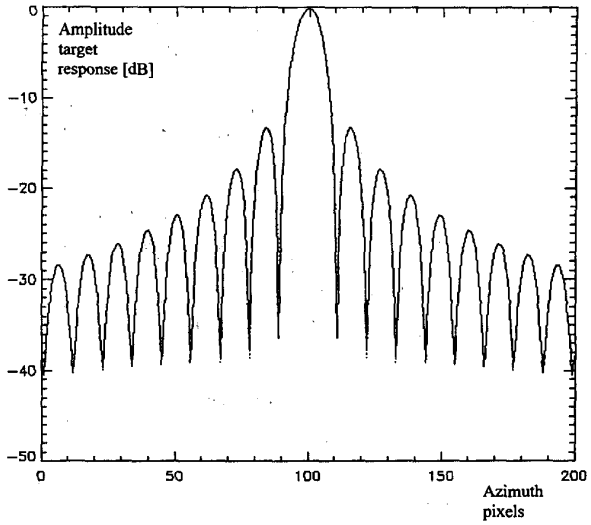

Fig. 12. Azimuth cut of nominal (continuous line) and motion compensated (dotted line) center range target response.

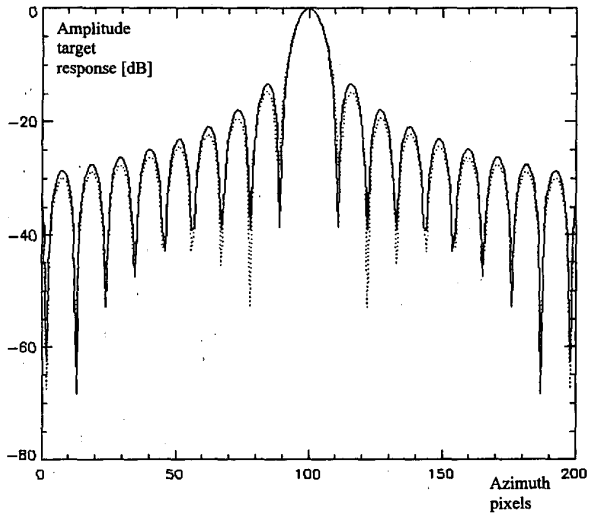

Fig. 13. Azimuth cut of nominal (continuous line) and motion compensated (dotted line) near range target response.

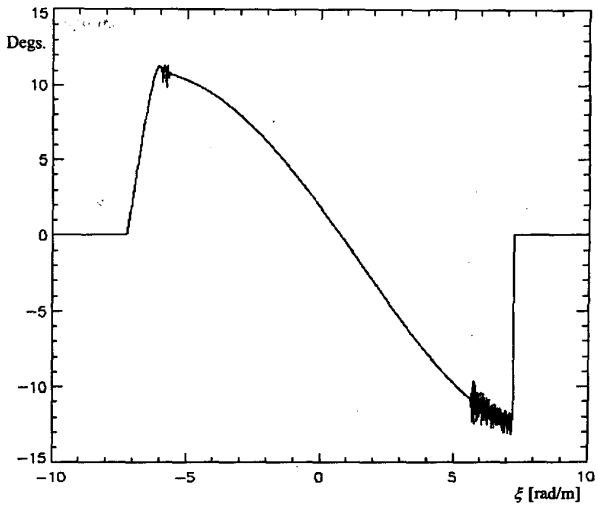

Fig. 14. Phase distortion of approximation in (32) for far range target.

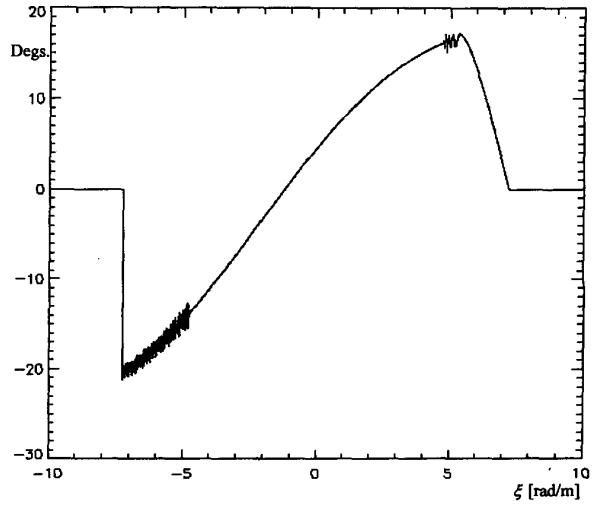

Fig. 15. Phase distortion of approximation in (32) for near range target.

VI. CONCLUSIONS

The paper presents a uniform treatment about the analysis and compensation of airplane deviation from the nominal trajectory in airborne SAR systems. It shows that trajectory displacements introduce replicas, along the azimuth frequency, of the raw data spectrum; these are weighted and integrated accordingly to the spectrum of the term associated with the displacements. Presence of this replication, beside the generation of geometric inaccuracies, induces a dispersion of the impulse response function that strongly impairs the quality of the focused image in terms of resolution loss. A description about the rationale of the MOCO procedures that are applied to reduce the impact of motion errors during the SAR processing is also addressed. Finally, the paper discusses the efficient integration of the MOCO within a standard two-dimensional Scaled-FT based SAR focusing code.

APPENDIX

Let $z(x')$ be a function expressed as follows:

$$z(x') = \int dx s s(x',x) u(x'-x) \tag{33}$$

wherein the integral is in $(-\infty,\infty)$. Equation (33) could represent the output to $s_1(x')$ of a "mild" space-variant linear system where the impulse response function $h(x',x'-x)$ can factorize in the

product $s_2(x')u(x'-x)$. Its FT gives

$$Z(\xi) = \iint dx'\,dx\,ss(x',x)u(x'-x)\exp[-j\xi x'] = \frac{1}{2\pi}\int dx\,Ss(\xi,x)\otimes_\xi [U(\xi)\exp(-j\xi x)] \quad (34)$$

which can be rearranged as follows:

$$Z(\xi) = \frac{1}{2\pi}\int d\zeta\,SS(\zeta,\xi-\zeta)U(\xi-\zeta) \quad (35)$$

wherein $SS(\cdot)$ is the FT of $ss(\cdot)$ along x' and x, and $\otimes_\xi$ denotes the convolution along ξ. Equation (10) follows from (35) by setting $ss(x',x) = q(x',r)\gamma(x,r)$ and

$$u(x'-x) = w^2(x'-x)\text{rect}\left[\frac{\eta}{2\Omega_r}\right] \times \exp[-j(\eta+4\pi/\lambda)(R_n-r) + j\alpha_\eta\eta^2] \quad (36)$$

that is the range FT of the SAR impulse response (before the focusing operation) function.

ACKNOWLEDGMENTS

The author wishes to tank Domenico Marzilli for implementing part of the numerical code, Riccardo Lanari and Eugenio Sansosti for interesting discussions about the topic, and Dr. Paul Lundgren of JPL for supporting the language revision of the paper.

REFERENCES

[1] Franceschetti, G., and Schirinzi, G. (1990)
A SAR processor based on two-dimensional FFT codes.
IEEE Transactions on Aerospace and Electronic Systems, **26** (Mar. 1990), 356–365.

[2] Raney, R. K., Runge, H., Bamler, R., and Cumming, I. G. (1994)
Precision SAR processing using chirp scaling.
IEEE Transactions on Geoscience and Remote Sensing, **32** (July 1994), 786–799.

[3] Franceschetti, G., Lanari, R., and Marzouk, S. (1996)
A new two-dimensional squint mode SAR processor.
IEEE Transactions on Aerospace and Electronic Systems, **32** (Apr. 1996), 854–863.

[4] Lanari, R., (1995)
A new method for the compensation of the SAR range cell migration based on the chirp Z-transform.
IEEE Transactions on Geoscience and Remote Sensing, **33** (Sept. 1995), 1296–1299.

[5] Lanari, R., and Fornaro, G. (1997)
A short discussion on the exact compensation of the SAR range-dependent range cell migration effect.
IEEE Transactions on Geoscience and Remote Sensing, **35** (Nov. 1997), 1446–1452.

[6] Blacknell, D., Freeman, A., Quegan, S., Ward, I. A., Finley, I. P., Oliver, C. J., White, R. G., and Wood, J. W. (1989)
Geometric accuracy in airborne SAR images.
IEEE Transactions on Aerospace and Electronic Systems, **25** (Mar. 1989), 241–258.

[7] Oliver, C. J. (1989)
Review article—Synthetic-aperture radar imaging.
Journal of Phys. D: Applied Physics, **25** (1989), 871–890.

[8] Buckreuss, S. (1991)
Motion errors in airborne synthetic aperture radar system.
European Transactions On Telecommunications, **2** (Nov.–Dec. 1991), 55–64.

[9] Moreira, J. (1990)
A new method of aircraft motion error extraction from radar raw data for real time motion compensation.
IEEE Transactions on Geoscience and Remote Sensing, **28** (July 1990), 620–626.

[10] Wahl, D. E., Eichel, P. H., Ghiglia, D. C., and Jakowatz, C. V., Jr. (1995)
Phase gradient autofocus—A robust toll for high resolution SAR phase correction.
IEEE Transactions on Aerospace and Electronic Systems, **30** (July 1995), 827–835.

[11] Werness, S. A., Carrara, W. G., Joyce, L. S., and Franczak, D. B. (1990)
Moving target imaging algorithm for SAR data.
IEEE Transactions on Aerospace and Electronic Systems, **26** (1990), 57–67.

[12] Wood, J. W. (1988)
The removal of azimuthal distortion in SAR images.
International Journal on Remote Sensing, **9** (1988), 1097–1107.

[13] Isernia, T., Pascazio, V., Pierri, R., and Schirinzi, G. (1996)
Synthetic aperture radar imaging from phase corrupted data.
IEE Proceedings—Radar, Sonar, Navigation, **143** (Aug. 1996), 268–274.

[14] Oliver, C., and Quegan, S. (1998)
Understanding Synthetic Aperture Radar Images.
London: Artech House, 1998, 43–73.

[15] Kirk, J. C. (1975)
Motion compensation for synthetic aperture radar.
IEEE Transactions on Aerospace and Electronic Systems, **11** (May 1975), 338–348.

[16] Farrell, J. L., Mims, J. H., and Sorrell, A. (1973)
Effects of navigation errors in maneuvering SAR.
IEEE Transactions on Aerospace and Electronic Systems, **9** (Sept. 1973), 758–776.

[17] Madsen, S. N., Zebker, H. A., and Martin, J. (1993)
Topographic mapping using radar interferometry: Processing and techniques.
IEEE Transactions on Geoscience and Remote Sensing, **31** (Jan. 1993), 246–256.

[18] Moreira, A., and Huang, Y. (1994)
Airborne SAR processing of highly squinted data using a chirp scaling approach with integrated motion compensation.
IEEE Transactions on Geoscience and Remote Sensing, **32** (Sept. 1994), 1029–1040.

[19] Moreira, A., Mittermayer, J., and Scheiber, R. (1996)
Extended chirp scaling algorithm for air- and spaceborne SAR data processing in stripmap and ScanSAR imaging modes.
IEEE Transactions on Geoscience and Remote Sensing, **34** (Sept. 1996), 1123–1136.

[20] Fornaro, G., and Franceschetti, G. (1995)
Image registration in interferometric SAR processing.
IEE Proceedings—Radar, Sonar, Navigation, **142** (Dec. 1995), 313–320.

[21] Carlson, A. B. (1986)
Communication Systems (3rd ed.).
Singapore: Mc-Graw Hill International, 1986, 236–241.

[22] Abramovitz, M., and Stegun, I. A. (1970)
Handbook of Mathematical Functions.
New York: Dover, 1970, 358–361.

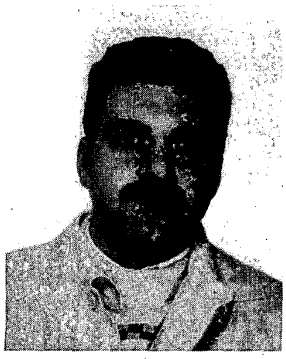

Gianfranco Fornaro received the Laurea degree in electronic engineering from the University of Napoli in 1992 and the Ph.D. degree from the University of Rome "La Sapienza" in 1997.

He is a full researcher at the Istituto di Ricerca per l'Elettromagnetismo e i Componenti Elettronici (IRECE) an institute of the Italian National Research Council (CNR) and Adjunct Professor of Signal Theory at the University of Reggio Calabria. His main research interests are in SAR data processing, SAR interferometry, and differential SAR interferometry. He has collaborated with the German Aerospace Establishment (DLR) for interferometric processing of airborne and spaceborne SAR data and has been a lecturer at the Istituto Tecnologico de Aeronautica (ITA) in Brasil.

Dr. Fornaro was awarded the Mountbatten Premium by the Institution of Electrical Engineers (IEE) in 1997.